On using variable molecular masses in multicomponent lattice Boltzmann simulations

Van den Akker, Harry E.A.; Donkers, Renske; Zachariah, Githin T.; Shardt, Orest

DOI
10.1016/j.jocs.2021.101432

Publication date
2021

Document Version
Final published version

Published in
Journal of Computational Science

Citation (APA)
Van den Akker, H. E. A., Donkers, R., Zachariah, G. T., & Shardt, O. (2021). On using variable molecular masses in multicomponent lattice Boltzmann simulations. *Journal of Computational Science*, *54*, Article 101432. https://doi.org/10.1016/j.jocs.2021.101432

Journal of Computational Science 54 (2021) 101432

Contents lists available at ScienceDirect

Journal of Computational Science

journal homepage: www.elsevier.com/locate/jocs

On using variable molecular masses in multicomponent lattice Boltzmann simulations

Harry E.A. Van den Akker [a,b,*], Renske Donkers [b], Githin T. Zachariah [a,b], Orest Shardt [a]

[a] Bernal Institute, School of Engineering, University of Limerick, Limerick, Ireland
[b] Transport Phenomena Group, Dept. of Chemical Engineering, Faculty of Applied Sciences, Delft University of Technology, Delft, Netherlands

ARTICLE INFO

Keywords:
Lattice Boltzmann
Multicomponent
Variable speed of sound
Droplet formation
Tubular reactor

ABSTRACT

The option of varying the molecular mass in multicomponent lattice Boltzmann simulations is being explored. First, results are presented for droplet formation at an aperture in a second immiscible liquid medium in which the difference in density between the two media is achieved by introducing asymmetry in the EOS, via adding particularly intra-component interaction forces in a pseudo-potential LB model. The second application for models with variable molecular masses is a single-phase heterogeneous laminar-flow tubular chemical reactor, where the molecular masses of reactants and products differ. In this application, tuning the molecular mass requires modification of the standard equilibrium distribution function as well as the use of an extended velocity set, in our case D2Q13. The method is validated against analytical solutions for canonical 1-D diffusion-reaction cases. In both the droplet formation study and the chemical reactors, the results of the exploratory 2-D simulations look qualitatively correct.

1. Introduction

In lattice Boltzmann (LB) simulations [1], fluids are represented by a finite number of parcels of molecules. These parcels travel across the simulation domain, each in a particular discrete direction from node to node of a specific lattice (grid); they assemble and interact at nodes, and then move on to the next node. The assembly of LB parcels (also called populations) at a node represents a (discretized) velocity distribution. The number of molecules in each parcel, *i.e.* its density f_i, may change at a node only, due to collisions (during which mass and momentum remain conserved) and/or forces. After such a rearrangement, the LB parcels take off, each departing in its own direction thereby transporting a modified part of the velocity distribution. More elaborate descriptions of this meso-scale type of simulation technqiue can be found elsewhere [1,2]. The standard LB technique solves a simplified and discretized Boltzmann equation that describes the spatio-temporal evolution of these densities f_i.

Thanks to the use of a proper lattice and proper collision rules – in this work, we use the conventional BGK approach to modelling collisions – this discretized Boltzmann equation quantitatively reproduces flow fields obeying the Navier-Stokes equation in the limit of long wave lengths (long with respect to the lattice scale). This restriction is usually formulated in terms of a Mach number $\mathrm{Ma} = u/c_s$ which should be (much) smaller than unity, where u denotes the fluid velocity and c_s is the speed of sound.

The above populations f_i as well as pressure perturbations propagate across the LB lattice, mutually connected by the velocity of sound c_s. As a matter of fact, this c_s plays a key role in LB models, since pressure, temperature and kinematic viscosity are all proportional to it. In addition, it sets a constraint in the Chapman-Enskog expansion towards the Navier-Stokes equation [1]. On several of the most commonly used lattice types, among which D2Q9 used in this study, c_s can be found [3] to be given by $c/\sqrt{3}$, in which the lattice velocity $c = \Delta x/\Delta t$ with Δx and Δt denoting the lattice spacing and the time step, respectively. The usual choice is to take Δx and Δt equal to unity (in l.u., lattice units) turning the numerical value of c_s equal to $1/\sqrt{3}$. In many LB simulations, c_s is treated as a constant.

From a physics standpoint, there are systems where this is not good because c_s is related to the (isothermal) compressibility of the fluid at hand. When using LB for simulating the flow of incompressible fluids, a velocity of sound c_s is not a physically meaningful or relevant variable, as strictly speaking sound propagation is impossible in an incompressible fluid. Yet, incompressible flow is being simulated by means of LB, by ensuring that the above Mach number is sufficiently low, with sound

* Corresponding author at: Bernal Institute, School of Engineering, University of Limerick, Limerick, Ireland.
E-mail addresses: harry.vandenakker@ul.ie, h.e.a.vandenakker@tudelft.nl (H.E.A. Van den Akker).

https://doi.org/10.1016/j.jocs.2021.101432
Received 31 January 2021; Received in revised form 17 June 2021; Accepted 15 July 2021
Available online 14 August 2021

propagation also being considered as just a weakly compressible phenomenon (see e.g., [1], p.111). Note however that sound propagation is not our topic of interest – we focus on the role of the numerical parameter 'speed of sound' c_s in any LB simulation due to its connection to the fluid's equation of state.

The speed of sound c_s, or the fluid's compressibility, is a physical property varying with temperature and – particularly relevant in this paper – with reciprocal molecular mass m, for an ideal component according to

$$c_s^2 = \left.\frac{\partial p}{\partial \rho}\right|_T = \frac{RT}{m} \tag{1}$$

To simulate the flow behaviour of multiple fluid components with different compressibility, Eq. (1) teaches us that we should be capable of varying, or tuning, the speed of sound for each individual component.

Buick and Cosgrove [4] were among the first or recognize that to model fluids with different compressibility changing the speed of sound is really required. Earlier, Alexander et al. [5] had altered the equilibrium distribution function in LB (see further on) while Yu and Zhao [6] had introduced an attractive force with the view of varying the speed of sound. Buick and Cosgrove [4] also added a body force to the Boltzmann equation. They all were capable of successfully applying c_s values between zero and, in the case of Buick and Cosgrove [4], even 1.125. While Alexander et al. [5] found also viscosity was affected by his method of varying the speed of sound, the forcing methods of Yu and Zhao [6] and Buick and Cosgrove [4] produced a variable c_s without affecting viscosity. All these authors were investigating non-linear aspects of sound-wave propagation. These papers, however, are of limited relevance for the current cases of interest, viz. incompressible multiphase and reactive flows where the multiple components exhibit varying compressibility due to varying molecular masses.

In (isothermal) multi-component systems such as emulsions, in diffusion processes inside binary mixtures, and in chemically reactive systems, the various miscible or immiscible components and reactants vary in molecular mass and therefore, given Eq. (1) for compressibility, may require the use of individual speeds of sound when being simulated by means of LB techniques. McCracken and Abraham [7] adjusted the speed of sound when simulating the behaviour of multiple components in diffusive mass transfer, while Arcidiacono et al. [8] and Bardow et al. [9] adopted multi-speed models for LB simulations of chemical reactions. All these authors explored, for systems without flow, the use of off-lattice schemes which allow components to travel just fractions of the lattice spacing during a lattice time step, depending on their relative molecular masses. For simulating flows, Chai and Zhao [10] and Looije et al. [11] investigated a variable speed of sound model involving a modified equilibrium distribution function on a D2Q13 lattice and by doing so recovered correct hydrodynamics.

Immiscible multi-component systems are very often simulated by the Pseudo-Potential (PP) LB model originally proposed by Shan & Chen [12,13]. In studies on PP LB methods, much attention is paid to the roles of the inter-component interaction strength G between the components that accounts for the degree of (im)miscibility of the components and spontaneous phase separation (if applicable), the Equation of State (EOS) for intra-component phase behaviour, and the choice between multiple relaxation times and a single relaxation time. In addition, the (isothermal) speed of sound, c_s, is a fourth essential but less often varied parameter.

The scope of this paper is then to explore various ways of varying this c_s in PP LB simulations of isothermal multi-component flow systems where the various components have a different molecular mass and therefore a different compressibility. We restricted ourselves to rather simple modifications of the multi-component PP LB model enabling simulations of multiphase flows with a phase interface and unequal phase densities as well as improved simulations of reactive single-phase systems. This paper now presents first exploratory results of varying the speed of sound for two cases, *viz.*

(A) droplet formation at an aperture in an immiscible second liquid, and
(B) simple chemically reactive single-phase flow systems.

These two approaches are novel to the best of our knowledge. They are rather different but both show viable options for dealing with cases where we really require deviations from the standard $c_s^2 = \frac{1}{3}$. In both cases, we stick to a single relaxation time LB model for the time being.

Before reporting about our explorations of varying molecular masses, and therefore also different speeds of sound, we will first summarise the basic equations of the PP LB model.

2. Summary of the PP LB model

The standard LBM solves a simplified and discretized Boltzmann equation that describes the spatio-temporal evolution of a parcel:

$$\frac{f_i(\vec{x} + \vec{e}_i\,\Delta t,\ t + \Delta t) - f_i(\vec{x},\ t)}{\Delta t} = -\frac{1}{\tau}\left[f_i(\vec{x},\ t) - f_i^{eq}(\vec{x},\ t)\right] + S_i \tag{2}$$

where f_i is the parcel density associated with the discrete velocity $\vec{e}_i$ and Δt is the time interval taken equal to 1 l.u. (as usual). The LHS stands for the streaming step during which f_i travels to an adjacent node, while τ at the RHS denotes the relaxation time of the process in which f_i adapts to the local equilibrium distribution function f_i^{eq} upon arrival at the new node. This discretized f_i^{eq} is given by

$$f_i^{eq} = w_i\rho\left[1 + \frac{\vec{e}_i\cdot\vec{u}^{eq}}{c_s^2} + \frac{(\vec{e}_i\cdot\vec{u}^{eq})^2}{2c_s^4} - \frac{\vec{u}^{eq}\cdot\vec{u}^{eq}}{2c_s^2}\right] \tag{3}$$

where $\vec{u}^{eq}$ is the equilibrium velocity and w_i are the weighting factors accounting for the spacing between the adjacent nodes in the D2Q9 lattice: 4/9 for $i = 0$, 1/9 for $i = 1$–4 and 1/36 for $i = 5$–8. The source term S_i in the RHS of Eq. (2) comprises all thermodynamic and hydrodynamic forces acting on the parcels at a lattice node. The spatial distributions of the continuum density and velocity are calculated from the LB variables via

$$\rho = \sum_i f_i \quad \text{and} \quad \rho\vec{u} = \sum_i \vec{e}_i f_i \tag{4}$$

A particular aspect of LB simulations is that the LB parameters must be chosen such that the computations simulate what is happening in the real, continuum world. The similarity rule is due to non-dimensional numbers in LB and in continuum space, such as the Reynolds number, which must bridge the gap between the two worlds by keeping them the same. Part of this procedure is that the above relaxation time τ is related to the kinematic viscosity ν of the fluid of interest according to

$$\tau = \frac{\nu}{c_s^2} + \frac{1}{2}\Delta t \tag{5}$$

Eq. (5) sets bounds to the permissible values of τ ; τ cannot be lower than 0.5 (for $\Delta t = 1$ ts).

In the Pseudo-Potential (PP) LB model description of multi-component multi-phase flows, next to *e.g.*, a body force $\vec{F}_b$ such as gravity, the mean-field inter-component force $\vec{F}_{\text{int}}$ plays an essential role in controlling (im)miscibility and spontaneous phase separation. In the original PP model [13], this interaction force is represented in terms of pseudo-potential functions Ψ_α and Ψ_β for the respective components α and β, the distribution functions of which are calculated each on its own lattice. In addition, the interaction force comprises an additional model parameter, *viz.* the interaction strength $G_{\alpha\beta}$:

$$\vec{F}_{\text{int}} = -G_{\alpha\beta}\,\Psi_\alpha(\vec{x},t)\,c_s^2\sum_i w_i\Psi_\beta(\vec{x}+e_i\Delta t) \tag{6}$$

For positive values of $G_{\alpha\beta}$, the interaction force $\vec{F}_{\text{int}}$ is repulsive, while it is attractive for negative values of $G_{\alpha\beta}$. All relevant forces, *e.g.* $F = \vec{F}_{\text{int}} + \vec{F}_b$, are used to calculate $\vec{u}^{eq}$ for use in Eq. (3) according to

$$\vec{u}^{eq} = \vec{u} + \frac{\Delta t}{2\rho}\vec{F} \tag{7}$$

Given this PP LB model described above in a nutshell, we now can report on our exploratory studies on varying the speed of sound.

3. Case A - Drop formation at an aperture

3.1. Introducing the case

Berghout and Van den Akker [14] simulated drop formation at an aperture by means of a two-component PP LB model, with the simplest assumption that the two pseudopotential functions equal the respective fluid densities and with a mutual interaction strength $G_{\alpha\beta}$ taken equal to 1.25. While the two components had equal densities and equal viscosities, gravity was allowed to work on the fluid (liquid) of the droplet only and to force this fluid out of the aperture, *i.e.* mimicking a liquid droplet in a gas. This was accomplished by putting specific weight $\gamma = \rho g$ equal to zero for the gas. As a result, the two components behave as two different phases.

Their 2-D results were in convincing qualitative agreement with literature data and demonstrated the effects of varying the non-dimensional numbers Ohnesorge $\text{Oh} = \mu/\sqrt{\rho D\gamma}$ and Archimedes $\text{Ar} = \rho g\Delta\rho D^3/\mu^2$, where γ denotes interfacial tension, μ stands for viscosity, ρ for density, $\Delta\rho$ for the density difference, g for gravity and D for droplet diameter. A plot of Capillary number $\text{Ca} = \mu v/\gamma$ versus Bond number $\text{Bo} = g\Delta\rho D^2/\gamma$ from the simulations coincided with the prediction on the basis of a simple dimensional analysis.

Now, we let gravity more realistically work on both components, though at a rather low density ratio simulating droplet formation in an ambient immiscible liquid. Mukherjee et al. [15] reported results for a density ratio between the components of 1.4, also in the presence of a surfactant as a third component. Our proposition in the current exploratory study is to obtain such a (low) density ratio by means of a variable speed of sound for (at least) one of the components and to find the maximum attainable density ratio. We keep the viscosity of the two components equal.

3.2. A standard EOS

In the single-component PP LB approach [12–14,16], the EOS for the bulk of a fluid is given by

$$p = c_s^2\rho + \tfrac{1}{2}\,c_s^2\Delta t^2 G\,\psi^2(\rho) \tag{8}$$

showing the ideal gas term is augmented with an additional contribution, due to non-ideal molecular attractions, which allows for coexisting liquid and vapour ([1], p. 373). This EOS can be rewritten into

$$\psi(\rho) = \sqrt{\frac{2}{c_s^2\Delta t^2 G}\left[p(\rho) - c_s^2\rho\right]} \tag{9}$$

Substituting into Eq. (9) an arbitrary EOS for $p(\rho)$, such as the Redlich-Kwong, the Carnahan-Starling or the Peng-Robinson EOSs, results in non-ideal fluid behaviour including phase separation with liquid to vapour density ratios up to as high as 10^3.

For a two-component system consisting of components α and β, the EOS runs as (see e.g. [1], p. 385, or [16]):

$$p = c_s^2\rho^\alpha + c_s^2\rho^\beta + c_s^2\Delta t^2 G_{\alpha\beta}\psi^\alpha\psi^\beta \tag{10}$$

still with $c_s^2 = \frac{1}{3}$. Again, the last term of the RHS of Eq. (10) is responsible for the (automatic) phase separation between the two components. We still can choose different expressions for the potential function, such as $\psi = \rho$ or, as in our case, the commonly used exponential relation

$$\psi(\rho) = \rho_0\left[1 - \exp(-\frac{\rho}{\rho_0})\right] \tag{11}$$

for each of the two components. The left panel of Fig. 1 illustrates the typical symmetric behaviour of the set of Eqs. (10) and (11) by plotting how (bulk) pressure symmetrically depends on the component densities ρ^α and ρ^β for $G_{\alpha\beta} = 2.50$.

3.3. An asymmetric EOS

To induce a density ratio between the two phases at a specific (total) pressure, an EOS asymmetric in the components α and β is required. Simply introducing in Eq. (10) different values for c_s^2, or RT, for the two components would not only affect pressures of individual components, but also viscosity and the stability limits of the model: so, this first option is not very useful.

A second option would be to take different pseudo-potential functions for the two components, e.g. by choosing in Eq. (11) different values ρ_0 for the components denoted as ${\rho_0}^\alpha$ and ${\rho_0}^\beta$, and by substituting the two resulting different potential functions α and β, into Eq. (10). By running exploratory simulations, we explored the maximum attainable density ratio as a function of $G_{\alpha\beta}$, ${\rho_0}^\alpha$ and ${\rho_0}^\beta$. The initial state in these 2-D simulations was a domain rich in α immersed in an ambient fluid rich in β at an initial density of unity in both phases, after which the system was allowed to evolve towards the pertinent equilibrium state. In a series of these simulations, the values of $G_{\alpha\beta}$, ${\rho_0}^\alpha$ and ${\rho_0}^\beta$ were varied to investigate their effect on the eventual density ratio of the two phases. A maximum phase density ratio of 1.25 between such a droplet and the surrounding liquid was found with $G_{\alpha\beta} = 3$, ${\rho_0}^\alpha = 1000$ and ${\rho_0}^\beta = 0.3$.

These latter three values were then used in Eqs. (10) and (11) to construct the right panel of Fig. 1 which illustrates how in this option #2 pressure varies with ρ^α and ρ^β in a (slightly) asymmetric way, although the density ratio of 1.25 is not found (in the absence of an interfacial tension effect in Eq. (10)). Our conclusion was that this option was too restrictive to accomplish sufficiently high phase density ratios, even when it did not have an effect on viscosity and the stability limits of the model.

A third option for getting an asymmetric EOS in the components α and β would be adding one or two intra-component interaction terms to the EOS of Eq. (10) – see also Chen et al. [16] and Mukherjee et al. [15] – resulting in

$$p = c_s^2\rho^\alpha + c_s^2\rho^\beta + c_s^2\Delta t^2 G_{\alpha\beta}\psi_1^\alpha\psi_1^\beta + \frac{c_s^2\Delta t^2}{2}G_{\alpha\alpha}\left(\psi_2^\alpha\right)^2 + \frac{c_s^2\Delta t^2}{2}G_{\beta\beta}\left(\psi_2^\beta\right)^2 \tag{12}$$

in which the subscripts 1 and 2 denote different pseudo-potential functions to be used to calculate the inter-component and intra-component forces, respectively. Using different pseudo-potential functions for the two components again modifies only pressure and interaction. A droplet with a higher density than the outer liquid is achieved by using $G < 0$ for the self-interaction of the component dominant in the droplet phase and/or $G > 0$ for the component dominant in the outer phase.

An asymmetric effect of components in a mixture has also been considered by Ridl and Wagner [17] in a comprehensive investigation on mixtures of multiple Van der Waals fluids. Their work is based on a free-energy LB method in which the forcing stems from a gradient in the chemical potential rather than from pseudo-potential functions. Ridl and Wagner [17] described the energetic interaction between (two) components with the help of a geometric mixing rule in terms of the

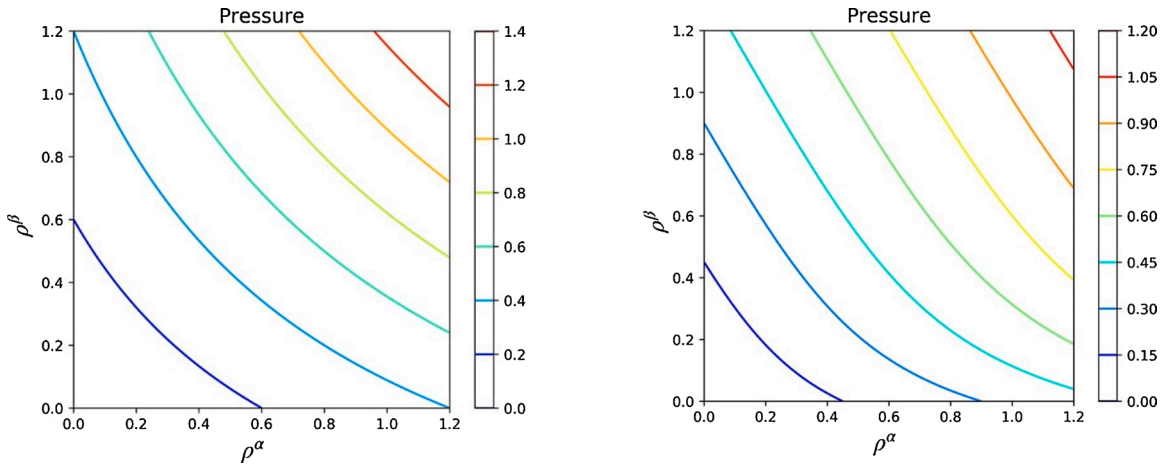

Fig. 1. Pressure as a function of component densities ρ^α and ρ^β according to the EOS of Eq. (10) along with Eq. (11): left panel: a symmetric EOS with $G_{\alpha\beta} = 2.50$ with the same ρ_0 for the two components; right panel: a (slightly) asymmetric EOS with $G_{\alpha\beta} = 3$, ${\rho_0}^\alpha = 1000$ and ${\rho_0}^\beta = 0.3$. The colour bar at the right-hand side of each panel refers to total pressure. The figures do not specify phase separation other than that the phases would be somewhere on the same isobar.

product of the respective Van der Waals attraction parameters rather than by an interaction strength $G_{\alpha\beta}$. The focus of their paper is on phase compositions and phase diagrams which is beyond our interest, as we are looking for a simple extension of the multi-component PP LB method allowing for a density difference between components.

Again, we ran simulations (now with a flat interface between two domains) to explore the effect of the various G values for the simple pseudo-potential function $\psi = \rho$. Now, we found higher phase density ratios such as 1.42 for $G_{\alpha\beta} = 1.25$, $G_{\alpha\alpha} = -0.3$, $G_{\beta\beta} = 0$ – illustrated in the left panel of Fig. 2 – and 1.92 for $G_{\alpha\beta} = 1.25$, $G_{\alpha\alpha} = -0.3$, $G_{\beta\beta} = 0.3$ – illustrated in the right panel of Fig. 2. Now, the degree of asymmetry is larger than in the right panel of Fig. 1. Furthermore, we found the inter-component interaction force not being affected in this option, the ideal terms in Eq. (12) being less dominant, and higher density ratios being attainable without simulations becoming unstable due to excessively strong forces.

3.4. Adjusting the speed of sound

Therefore we decided to use option 3 – i.e., Eq. (12) – when simulating drop formation at an aperture with a modest density difference between a liquid drop and ambient fluid. This option renders either or both components non-ideal resulting in intracomponent phase separation. To avoid this, rather than using $\psi = \rho$ or Eq. (11), we substitute $R\,\rho$ for p (ρ) in Eq. (9) for either or both components. The approach is illustrated by the following example: we substitute

$$\psi_1^\alpha = \rho^\alpha;\ \psi_1^\beta = \rho^\beta;\ \psi_2^\alpha = \sqrt{\frac{2}{c_s^2 \Delta t^2 G_{\alpha\alpha}}(R_\alpha \rho^\alpha - c_s^2 \rho^\alpha)}\ ;\ \psi_2^\beta = 0 \tag{13}$$

into Eq. (12) to arrive at

$$p = R_\alpha \rho^\alpha + \rho^\beta + c_s^2 \Delta t^2 G_{\alpha\beta} \rho^\alpha\ \rho^\beta \tag{14}$$

Then, Eq. (14) may be denoted as an adjusted speed of sound model comprising two ideal gas terms plus an inter-component interaction contribution. Due to the ideal gas behaviour of the two components, the model is kept simple with intra-component phase separation being prevented. This approach only modifies the EOS for the mixture. The ideal behaviour of component β can be modified in a similar way, on its own or in combination – see Eq. (12) – with that of component α. The EOS of the adjusted speed of sound model of Eq. (14) is visualised in Fig. 3 for two values of R_α lower than $c_s^2 = \frac{1}{3}$. The asymmetry is qualitatively rather similar to that in Fig. 2, implying that similar phase density ratios can be attained.

The values for the density ratio and the surface tension, which can be obtained by using the above adjusted speed of sound model, depend on the values of $G_{\alpha\beta}$ and R_α. Again, we carried out 2-D simulations for two phases separated by a flat interface, each with an initial density of unity. The maximum density ratio (see Fig. 4) amounted to 2.55 for $R_\alpha = 0.13$

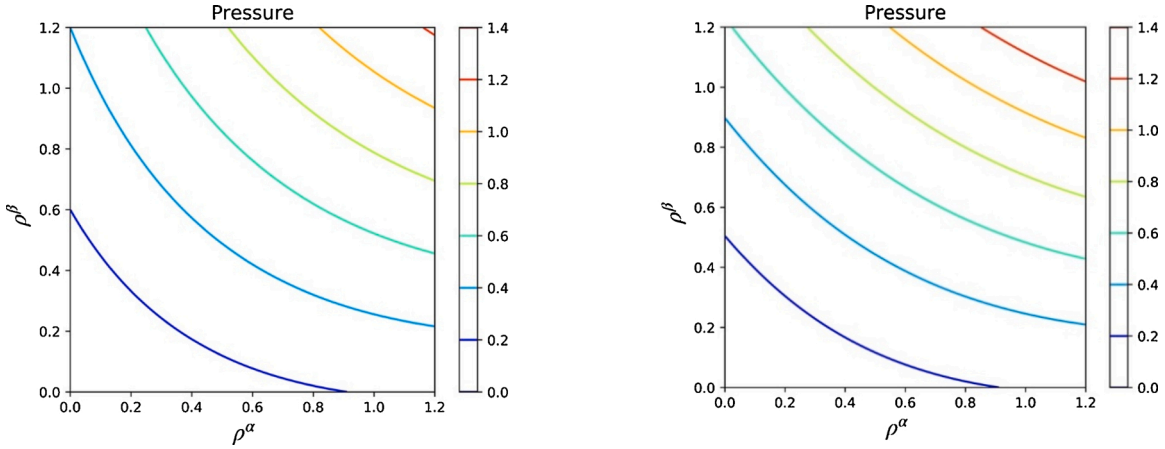

Fig. 2. Pressure as a function of ρ^α and ρ^β in option #3 according to the EOS of Eq. (12): left panel: with $G_{\alpha\beta} = 1.25$, $G_{\alpha\alpha} = -0.3$, $G_{\beta\beta} = 0$; right panel: with $G_{\alpha\beta} = 1.25$, $G_{\alpha\alpha} = -0.3$, $G_{\beta\beta} = 0.3$.

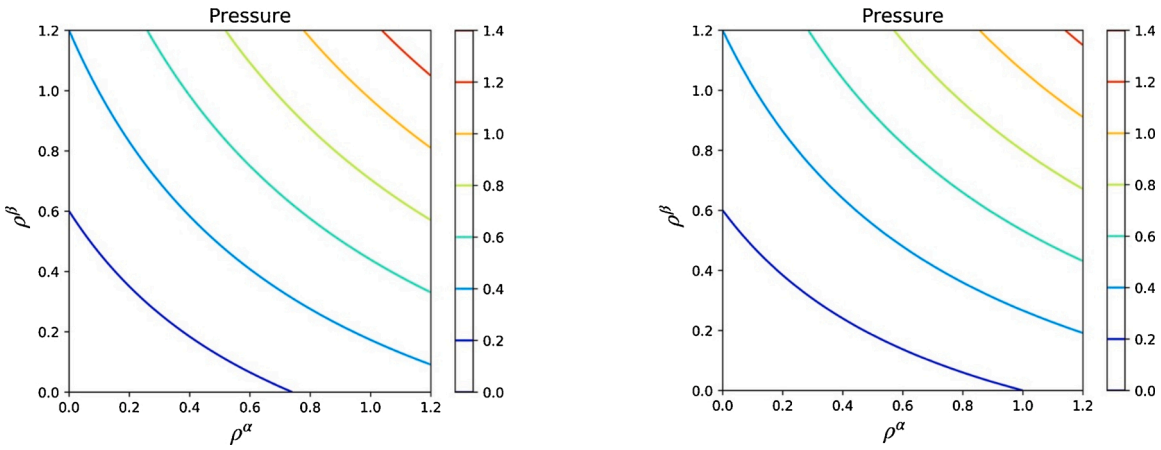

Fig. 3. Pressure as a function of ρ^α and ρ^β in the adjusted speed of sound model of Eq. (14): left: with $G_{\alpha\beta} = 1.25$ and $R_\alpha = 0.27$; right: with $G_{\alpha\beta} = 1.25$ and $R_\alpha = 0.20$.

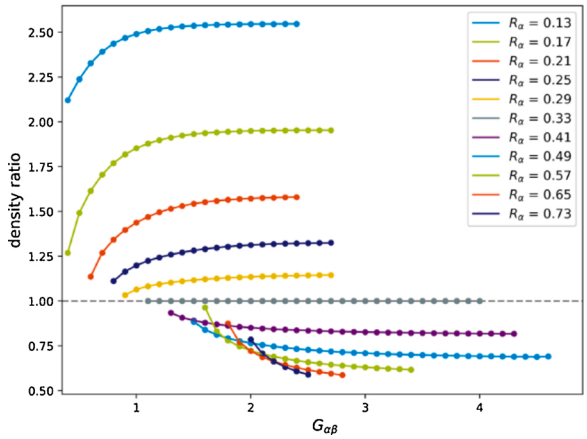

Fig. 4. The density ratio for the two phases (α rich over β rich), according to the adjusted speed of sound model of Eq. (14), as a function of $G_{\alpha\beta}$ and R_α.

with $G_{\alpha\beta}$ in the range 1.5–2.5; such $G_{\alpha\beta}$ values in this plateau are sufficiently high to induce almost complete phase separation as a result of which in the bulk of either phase either ρ^α or ρ^β is about zero rendering the last term of Eq. (14) more or less zero such that $\rho^\alpha/\rho^\beta = c_s^2/R_\alpha = 2.56$ indeed. The minimum value of the density ratio was about 0.60 for $R_\alpha = 0.73$ and $G_{\alpha\beta} = 2.5$; then, phase separation is not complete (no plateau in the curve yet) and the above simplification of Eq. (14) does not apply.

Fig. 4 also illustrates that $R_\alpha = 0.33 = c_s^2$ reproduces the ratio (with a flat interface) of unity. Reducing the value of R_α decreases the contribution of ρ^α to the pressure such that an equal pressure across the two phases requires the total density of the α rich phase to be higher than that of the β rich phase. Decreasing R_α further down than 0.13 and increasing it above 0.73 resulted in unstable simulations. Higher values of the density ratio may be attained when alongside R_α also an R_β is varied. This route has not yet been explored.

3.5. Running the simulations of drop formation

We then applied the adjusted speed of sound model of Eq. (14) to the topic of drop formation at an aperture as simulated before by Berghout and Van den Akker [14], the essential difference (and major step forward) being that gravity now acts on both components. As before, we restricted ourselves to a 2-D simulation for the sake of computational time and memory, while invoking the same justification as before, and used a D2Q9 velocity set. The relaxation time was taken equal to unity for both components, while neutral wetting conditions were set, again as before. While the earlier simulations were run within Palabos with an interface written in C++, the current model was implemented in Python without parallelisation. Initially, the heavier liquid 1 rich in component α was in the aperture and in the rather shallow domain above the plate with the aperture, while the β rich phase 2 was below. Gravity then pulls liquid 1 out of the aperture (of diameter D) downwards, pushing away the lighter liquid 2, to eventually form a droplet.

The rectangular computational domain had periodic conditions implemented on the vertical sides allowing outflow of fluid, while bounce-back rules imposed on the walls of the plate with the aperture. At the top of the computational domain, which was at some distance above the aperture plate, an open boundary condition was used with the densities of the top nodes copied to the fictive nodes above the domain. At the bottom of the lower domain ($z = 0$) a bounce-back rule was imposed to avoid outflow of both fluids through the domain bottom. To prevent compressibility effects, due to this bounce-back bottom, from creating pressure and density gradients along the height h of the domain (up to the aperture) and the pertinent additional unphysical flows, we imposed an initial density gradient very close to the equilibrium density gradient by applying

$$\rho(z) = \rho_0 \exp\left(-\frac{gz}{c_s^2}\right) \tag{15}$$

$$\text{with } \rho_0 = \frac{\rho_{av}\,\frac{gh}{RT}}{1 - \exp\left(-\frac{gh}{RT}\right)} \quad \text{and} \quad \rho_{av} = \frac{1}{h}\int_0^h \rho(z)dz \tag{16}$$

to both components except that for α the adjusted speed of sound R_α is used rather than c_s^2. In addition, we kept LB gravity as low as possible, although the Bond number should remain of the order of unity. This requires a subtle search for the proper LB values for the physical properties and the geometrical parameters to arrive at non-dimensional Bond (Bo), Archimedes (Ar) and Ohnesorge (Oh) numbers allowing droplet pinch-off.

The other question is which value of R_α would be optimal given our Fig. 4. After all, we ended up with $R_\alpha = 0.15$, $g = 0.000374$, an aperture 44 nodes in width and 50 nodes in height, with a 50 nodes thick layer of liquid 1 above the aperture, and a domain height of 1000 lattice nodes below the aperture. Table 1 presents the conditions of the three simulations A1–A3 accomplished. Just like in the earlier work [14], the fluid velocity in the aperture and hence also the Reynolds number are the result of the simulation. Given the lattice density and numbers of time steps in excess of 10^5, each simulation took 3–5 days.

Table 1
The three simulations carried out with the adjusted speed of sound model of Eq. (14).

Case	$G_{\alpha\beta}$	ρ_1/ρ_2	$\Delta\rho/\gamma$	*Bo*	*Ar*	*Oh*
A1	0.40	1.69	11.6	0.83	46	0.13
A2	0.30	1.53	14.6	1.05	39	0.16
A3	0.25	1.45	16.7	1.20	35	0.18

3.6. Some simulation results

A typical result of a simulation on the basis of an adjusted speed of sound ($R_\alpha = 0.15$) is presented in Fig. 5, viz. case A1. As the non-dimensional numbers Bo, Ar and Oh of the three cases of Table 1 are rather different from those presented in our earlier paper [14], the time series is not one-to-one comparable with the earlier results. Yet, the results look qualitatively correct as far as *e.g.*, neck elongation, pinch-off, transient droplet shape and retracting neck filament are concerned.

Fig. 6(a)-(c) exhibit the non-dimensional wetted diameter D_i/D, the non-dimensional apex distance L/D, and the non-dimensional minimum neck thickness $h_{\min}/D$ as a function of time for the three cases A1–A3. Again, compared to the earlier data [14], these curves show slightly different dynamics of droplet formation at different operating conditions, but overall the curves are rather similar. Of course, one may wonder whether the results, particularly the thinning of the neck and the eventual pinch-off time may suffer from inaccuracies due to issues such as lattice spacing and the diffuse phase interface typical of LB (see e.g. Mukherjee et al. [18]). Most provisos already made by Berghout and Van den Akker [14] apply here as well. These aspects need further study by means of 3-D simulations (although the resolution issue will remain anyhow).

3.7. Conclusions for Case A

We showed the potential of obtaining a density ratio between the two phases in a MC PP LB model by means of adjusting the speed of sound in (at least) one of the two phases, i.e., by replacing the square of the speed of sound c_s^2 in the ideal gas part of the EOS of one component by a variable R_α. One may argue that this approach is similar to adding a body force that cancels out $-\nabla(c_s^2\rho)$, replacing it with $-\nabla(R\rho)$. Given Eq. (14), we may describe the approach as an adjustable speed of sound model.

We found that the density ratio increased by increasing the difference between c_s^2 and R_α along with increasing the interaction strength $G_{\alpha\beta}$.The maximum density ratio that can be realised is limited to about 2.5 as large intracomponent forces arise for larger differences between c_s^2 and R_α resulting in unstable simulations. For the time being, we did not explore whether (how much) higher density ratios could be obtained by invoking adjusted speeds of sound for both components.

Simulations exploiting an adjusted speed of sound, viz. $R_\alpha = 0.15$, were run for three cases of droplet formation at an aperture with varying

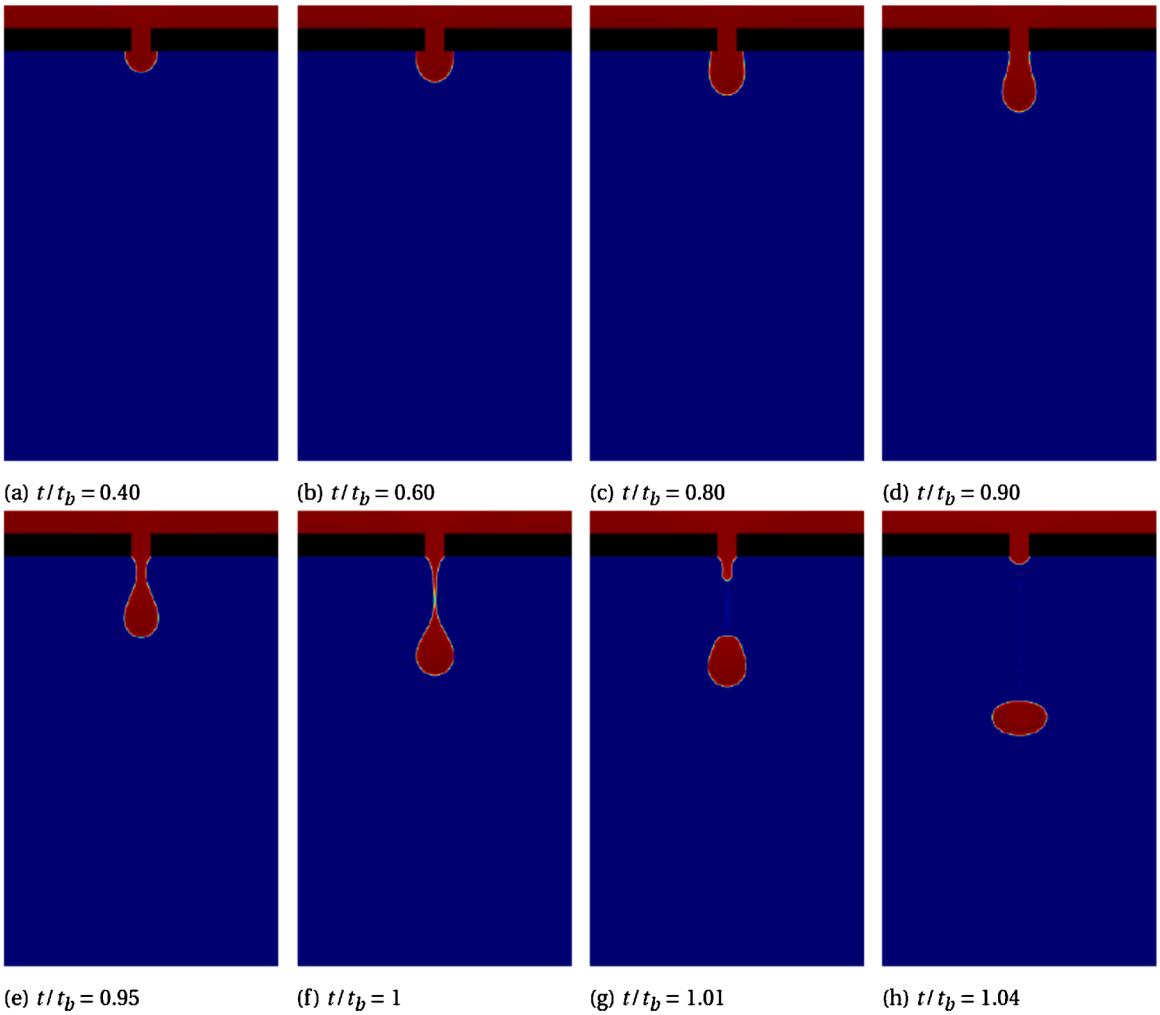

Fig. 5. Case A1: Droplet formation at an aperture as found by means of the adjusted speed of sound model of Eq. (14), t_b denoting the pinch-off of the droplet after (in this case) 146,500 time steps.

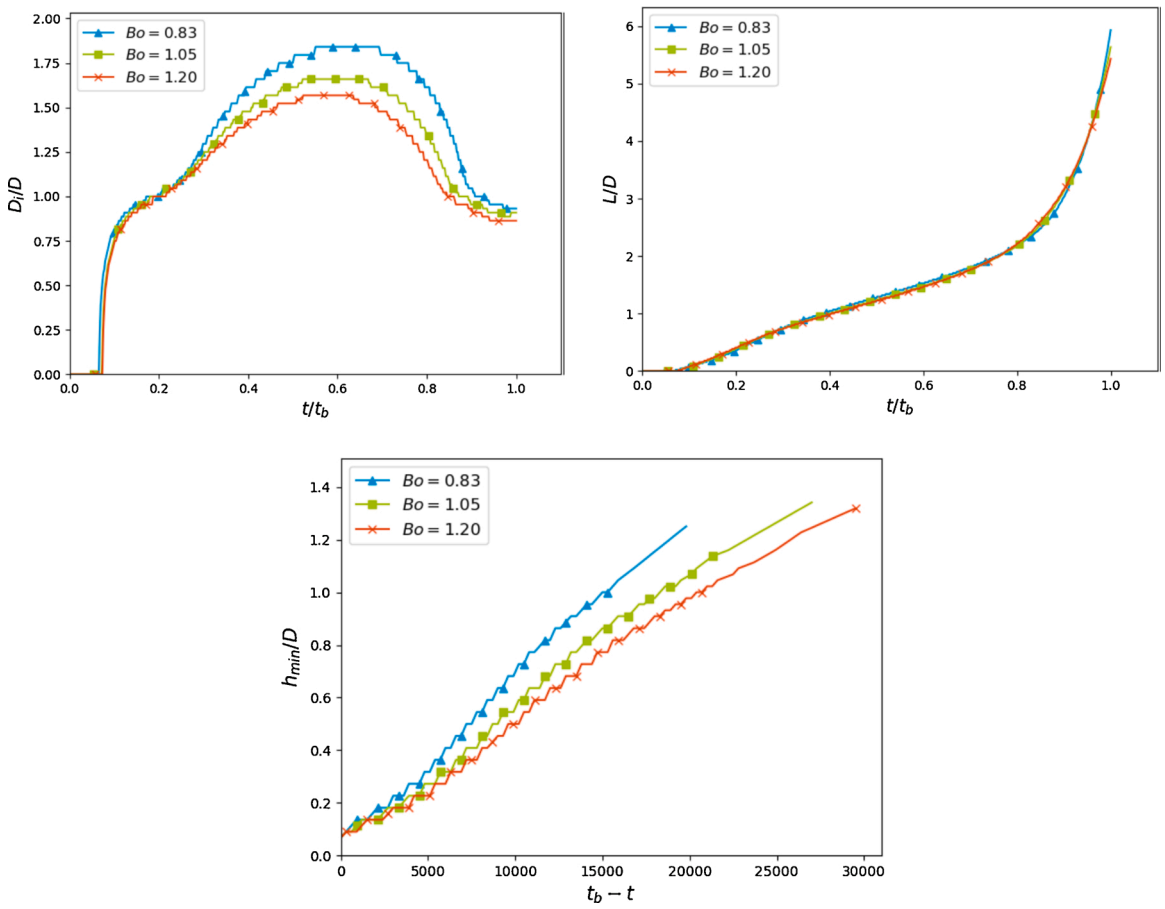

Fig. 6. (a) non-dimensional wetted diameter D_i/D, (b) the non-dimensional apex distance L/D and (c) the non-dimensional minimum neck thickness $h_{\min}/D$, all as a function of time for the three cases A1–A3, as found by means of the adjusted speed of sound model of Eq. (14).

Bo, Ar and Oh numbers. The results were encouraging as they showed qualitatively correct physics of droplet formation. A quantitative comparison of these exploratory findings with earlier results such as those reported by Berghout and Van den Akker [14] and other authors such as Pozrikidis [19] is not doable due to (a) deviating operating conditions in terms of non-dimensional Bo, Ar and Oh numbers, and (b) the restriction to 2-D of the current exploratory simulations.

4. Case B - Tubular chemical reactors

4.1. Introducing the case

In chemical reactors, the reacting chemical species usually have different molecular masses and produce product species again with different molecular masses. As expressed by Eq. (1), each species, therefore, has a different speed of sound and the populations of each species may move at a different velocity across the lattice. Previously, several authors [7,8,10,11,20] have also appreciated this. In this Case B, the approach is essentially different from that in Case A, since now the actual lattice speed of sound is being modified. In addition, for these single-phase cases, we do not make use of the pseudo-potential model.

We now report about using such a variable speed of sound multi-component single-phase single-relaxation-time on-lattice LB model as proposed by Looije et al. [11] for simulating various heterogeneous reactive cases. For isothermal non-reactive flows, the latter authors showed that such a tunable speed of sound not only requires modification of the standard equilibrium distribution function (just like reported by *e.g.*, Alexander et al. [5] and Viggen [21]) but also the use of an extended velocity set: to avoid unphysical error terms in the Navier-Stokes equation. Although this was reported earlier by Qian [22] and by Chai and Zhao [10], Looije et al. [11] presented a full derivation of the pertinent relations for single-component cases. They also demonstrated, still for isothermal single-component fluids, that tuning the speed of sound along with using a modified equilibrium distribution and an extended velocity set (D2Q13) results in reproducing the proper flow characteristics of both a damped standing pressure wave and a decaying viscous Taylor-Green vortex. The advantages shown relate to an improved convergence rate and strongly reduced errors.

For each component, we therefore use a D2Q13 lattice with a common mixture velocity. The partial pressure of each component is calculated by using

$$p = c_{s,e}^2 \rho = \chi c_s^2 \rho \tag{17}$$

since, just like in Looije et al. [11], we introduce the tuning parameter χ for reducing or increasing the squared standard lattice speed of sound c_s with the view of reflecting the differences in molecular mass of reactants and products. Similarly, we redefine viscosity for each component as

$$\nu_e = \chi \nu = c_{s,e}^2 \Delta t \left(\frac{\tau}{\Delta t} - \frac{1}{2} \right) \tag{18}$$

For the derivation of the coefficients in the modified equilibrium distribution function we refer to the Appendix of Looije et al. [11].

For the LB simulation of the reaction A → *m*B at a catalytically active surface, we use the reactive bounce-back method introduced by Kamali et al. [23], also used by e.g., Ashorynejad et al. [24] for the cathode processes in a fuel cell. In this method, the fraction k_s^{LB} of A arriving at the surface is converted into B while the remaining fraction 1- k_s^{LB} still returns as A. Due to the use of the D2Q13 lattice, the LB surface reaction

rate constant had to be modified and is now given by

$$k_s^{LB} = \frac{96\, k_s \cdot \delta t}{21\, \delta z} \Big/ \left(1 + \frac{k_s \cdot \delta z}{2D}\right) \tag{19}$$

where the usual continuum variables k_s and D denote the surface reaction rate constant and the diffusion coefficient, respectively.

We applied the above Looije approach to three reactive single-phase reactions and reactors as described in the Sections 4.2 through 4.4.

4.2. Between two flat plates skip indentation

A multicomponent 1-D diffusion-reaction case between two flat plates, one of which ($x = 0$) imposes a constant concentration of species A while at the other wall (x=L) a heterogeneous chemical reaction A → mB takes place, m being varied. When $m \neq 1$, the problem is to be described in terms of Stefan's law rather than as simple Fickian diffusion. We varied the Damköhler numer Da, defined as $k_s L/D$ and representing the ratio of surface reaction rate to diffusion rate. The analytical solution for the molar concentration c of component A for this case [25] runs as

$$m = 1 : \frac{c}{c_0} = 1 - \frac{Da}{Da + 1}\,\eta \tag{20a}$$

$$m > 1 : \frac{c}{c_0} = \frac{m \exp\,\{-[W\,(m\,Da \exp Da) - Da]\,\eta\,\}\text{-}\,1}{m - 1} \tag{20b}$$

in which $\eta = \frac{x}{L}$ and W is the Lambert W-function. For the purpose of validating our approach, we selected $m = 1$ and $m = 2$. In the latter case, the number of moles changes as a result of the reaction, while at the same time the molecular masses of A and B differ by a factor of 2. This is taken care of by adapting the tuning parameter χ : for $m = 2$, we took $\chi = 0.665$ for component A and $\chi = 1.33$ for B. In the simulations, we used 40 l.u. for the spacing between the two flat plates.

By plotting the non-dimensional concentration of A as a function of the spatial coordinate in l.u. for two reactions $m = 1$ and $m = 2$ with varying Da, Fig. 7 illustrates that our simulation results agree with the analytical solutions provided that for the $m = 2$ case the multi-speed approach is applied.

4.3. Laminar-flow tubular reactor skip indentation

A tubular reactor operated under laminar flow conditions with the reaction 2A → 3B taking place at the tube wall. We use $\chi = 0.8$ for reactant A and $\chi = 1.2$ for product B with the view of arriving at the stoechiometric ratio 3/2, while avoiding computational stability issues for χ values beyond 1.2. For the inlet of the tubular reactor, we extended the local Zhou-He boundary condition to D2Q13 lattices for both the velocity and the mass fractions of the components, while at the outlet we imposed a parabolic velocity profile by using a bounce back boundary condition. The corners of the flow domain need special treatment as they are at the intersection of the inlet (or outlet) plane and the tube wall where the reaction takes place.

Fig. 8 demonstrates a typical result for pressure field, x-velocity field and the concentration fields for the two components A and B from simulations for this case. Qualitatively, the results look acceptable, with the density at the outlet 0.7 as predicted from a pressure balance for complete conversion of A when using the above χ values and the inlet mass fractions 0.9 and 0.1 for A and B, respectively. The velocity increases in downstream direction due to the decrease in density as a result of the chemical reaction. Pressure is more or less constant, with still a few numerical artefacts close the wall in the first half of the reactor.

This case served the only purpose to explore whether the method works in a flow reactor, which boundary conditions are needed, whether the code is numerically stable, and whether meaningful results are obtained. We are not aware of experimental or computational literature data for this reaction and for these operating conditions which we could have used for validation.

4.4. Catalytic combustion of methane skip indentation

The catalytic combustion of methane $CH_4 + 2\,O_2 \rightarrow 2\,H_2O + CO_2$ in a tubular laminar-flow reactor with an L/D ratio of 10, as described in the paper by Arcidiacono et al. [8], with our simulation approach being essentially different in terms of type of lattice scheme (on-lattice *vs* off-lattice), boundary conditions, and the treatment of the heterogeneous reaction.

We used the same inlet and outlet boundary conditions as in the above case (b). Further, we selected the tuning parameters χ– see Eqs. (17) and (18) – for the various components as 1.6775, 0.8387, 0.61 and 1.4911 for methane, oxygen, CO_2 and water, respectively, by taking χ for the largest molecule equal to the lower stability limit (i.e., 0.61) and then considering the ratio of the molecular masses – see Eq. (1) – for the χ values of the other components.

In addition, some of our simulation conditions differed from Arcidiacono's: we used Re = Pe = 1, while our reaction started not earlier than $x = L/4$. Due to these differences, our results are not comparable

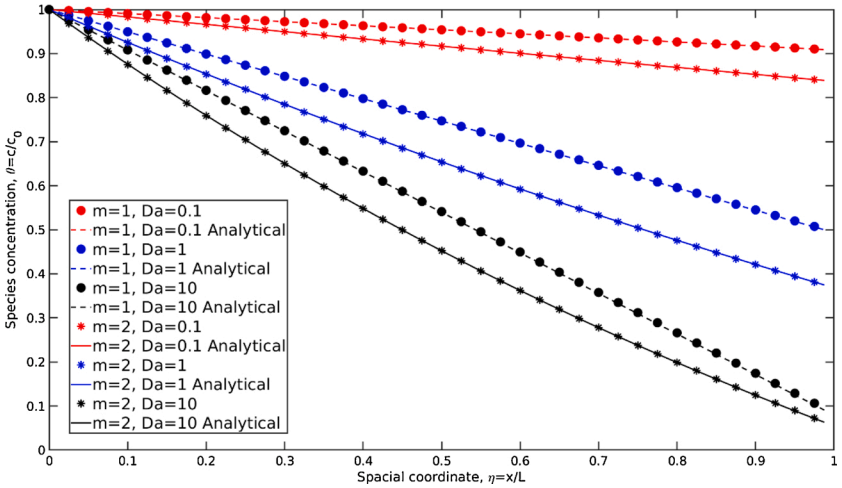

Fig. 7. Plot of non-dimensional concentration of component A versus the non-dimensional coordinate η for case A → B ($m = 1$) and A → 2B ($m = 2$): the different symbols represent the LB results, while the different lines are the analytical solutions of Eqs. (20). In the case $m = 2$, the speed of sound is tuned to reflect the difference in molecular mass of components A and B. In both plots, Da is an important parameter, as expected. The LB results match the analytical solutions.

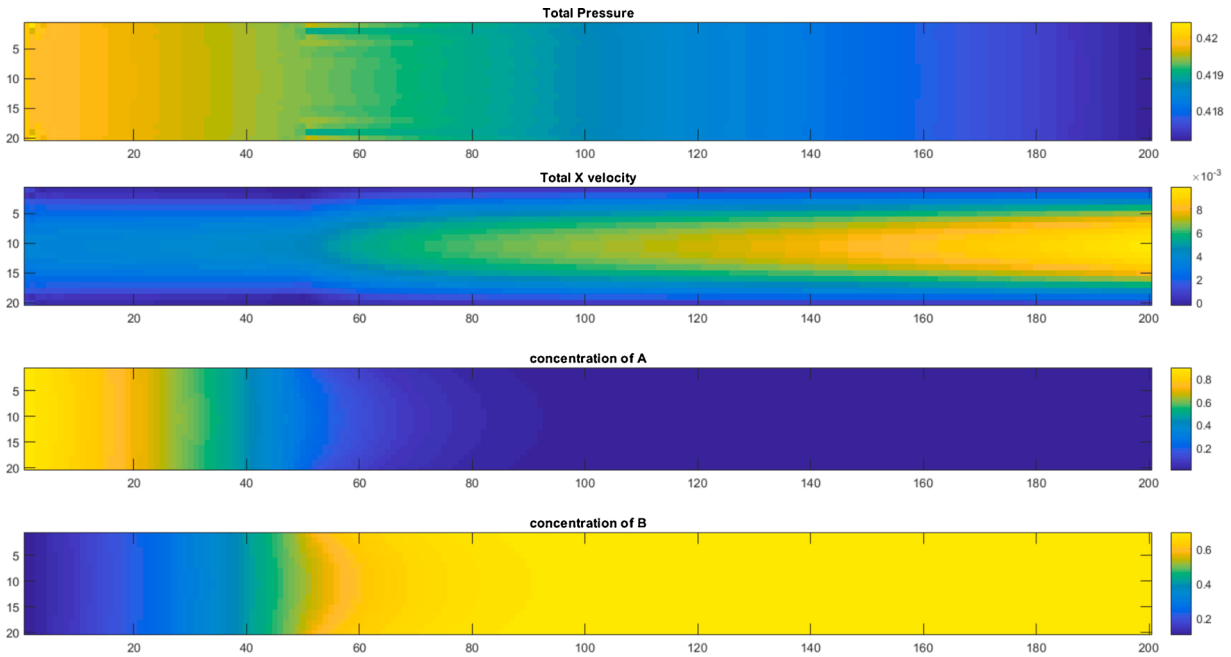

Fig. 8. 2-D simulation of a laminar flow reactor with surface reaction 2A→3B at the pipe wall for Re = Pe = 1 and Da = 1 in a domain of 20 × 200 l.u. Inlet mass fractions of components A and B were 0.9 and 0.1, respectively. Reaction starts at $x = L/4$.

with Arcidiacono's. We did use the same kinetic data to arrive at $k_s = 28$ cm/s which then was used to calculate k_s^{LB} by means of Eq. (19). We also used the same inlet mole fractions of methane and oxygen, but note that for our LB simulation we converted the mole based stoichiometry to mass based.

Fig. 9 presents the simulation results for the catalytic combustion of methane: pressure field, velocity field and the concentration fields of reactants and reaction products. The results look qualitatively correct. The velocity does not change in the downstream direction: this is different than in Fig. 8, as now the number of moles does not change as result of the reaction, while the molecular masses do vary. Fig. 10 shows the velocity profiles halfway the reactor which are qualitatively in agreement with the velocity profiles presented by Arcidiacono et al. [8] in their Fig. 6.

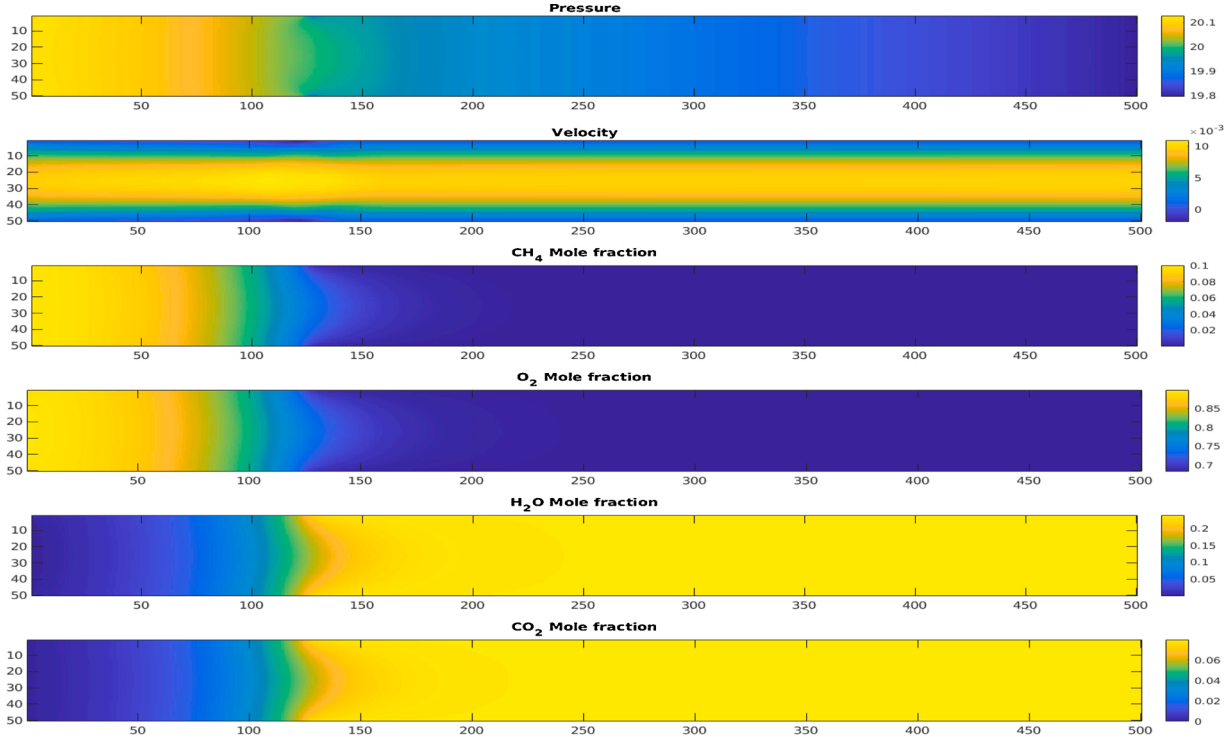

Fig. 9. 2-D simulation of the catalytic combustion of methane at the pipe wall for Re = Pe = 1 on a domain of 50 × 500 l.u. Inlet mole fractions of oxygen and methane were 0.9 and 0.1, respectively. Reaction starts at $x = L/4$.

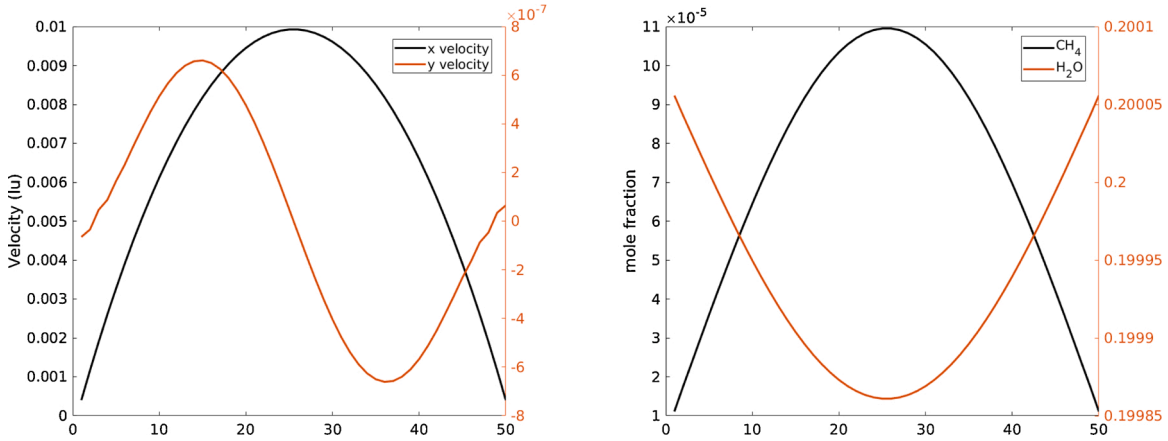

Fig. 10. Velocity profiles and mole fraction profiles halfway gthe reactor as found in a 2-D simulation of the catalytic combustion of methane at the pipe wall for Re = Pe = 1 on a domain of 50 × 500 lu. Inlet mole fractions of oxygen and methane were 0.9 and 0.1, respectively.

4.5. Conclusions for Case B

The three above cases show that the concept of varying the speed of sound after the molecular mass of the multiple components in a chemical reaction is not only physically necessary but also computationally feasible. The concept does require the use of an extended lattice, or extended velocity set, *i.e.*, D2Q13 instead of D2Q9, and a modified equilibrium distribution, as specified and validated for non-reactive cases by Looije et al. [11]. The method has the obvious drawback of an increased computational burden due to the extended lattice. While the method for reactive systems was properly assessed for the canonical 1-D case (a) by comparing with analytical solutions for varying Damköhler numbers, the 2-D results for the tubular reactors of cases (b) and (c) look qualitatively correct but need further quantitative validation by means of (literature) data from either experiments or different types of simulations.

5. Overall conclusions and outlook

The submission that varying the speed of sound is an underexposed but viable option in LB simulations of isothermal multicomponent systems was explored for both two-phase flow, *viz.* droplet formation at an aperture, and single-phase catalyst assisted chemical flow reactors. In the former case (A), adjusting the speed of sound for either or both components along with the use of pseudo potential functions turns out to be instrumental for obtaining phase separation with a modest phase density difference. In the latter case (B), tuning the speed of sound by taking differences in molecular mass into account is a more drastic modification as it interferes with core LB aspects as lattice size and equilibrium distribution functions.

By comparing with the analytical solutions for a simple 1-D diffusion-reaction case we demonstrated that tuning the speed of sound is really required when molecular mass is different for reactant and reaction product. Our 2-D simulations with varying speeds of sound produced qualitatively satisfactory results for droplet formation at an aperture, for a simple test reaction in a tubular reator and for catalytic combustion of methane in a tubular reactor.

The applicability of the two methods of varying the speed of sound should further be investigated, also in 3-D, and assessed for varying conditions for which literature dara are available. The two methods should also be extended by incorporating multiple relaxation times to reflect differences in Peclet numbers as a result of differences in molecular mass and size. Last but not least, a more detailed assessment of the effects of a variable speed of sound on the numerical stability of the pertinent LB codes is highly needed and strongly recommended.

Author contribution statement

All of the authors were involved in the preparation of the manuscript and have read and approved the final manuscript version.

Declaration of Competing Interest

The authors declare that they have no known competing financial interests or personal relationships that could have appeared to influence the work reported in this paper.

References

[1] T. Kruger, et al., The Lattice Boltzmann Method - Principles and Practice, Springer, 2017.
[2] H.E.A. Van den Akker, Preface, in: H.E.A. Van den Akker (Ed.), Lattice Boltzmann Modeling for Chemical Engineering, Vol. 55 of Advances in Chemical Engineering, Elsevier Academic Press, 2020, pp. ix–xxi.
[3] Y.H. Qian, D. Dhumieres, P. Lallemand, Lattice BGK models for Navier-Stokes equation, Europhys. Lett. 17 (6BIS) (1992) 479–484.
[4] J.M. Buick, J.A. Cosgrove, Investigation of a lattice Boltzmann model with a variable speed of sound, J. Phys. A-Math. Gen. 39 (44) (2006) 13807–13815.
[5] F.J. Alexander, et al., Lattice Boltzmann model for compressible fluids, Phys. Rev. A 46 (4) (1992) 1967–1970.
[6] H.D. Yu, K.H. Zhao, Lattice Boltzmann method for compressible flows with high Mach numbers, Phys. Rev. E 61 (4) (2000) 3867–3870.
[7] M.E. McCracken, J. Abraham, Lattice Boltzmann methods for binary mixtures with different molecular weights, Phys. Rev. E 71 (4) (2005).
[8] S. Arcidiacono, J. Mantzaras, I.V. Karlin, Lattice Boltzmann simulation of catalytic reactions, Phys. Rev. E 78 (4) (2008).
[9] A. Bardow, I.V. Karlin, A.A. Gusev, Multispeed models in off-lattice Boltzmann simulations, Phys. Rev. E 77 (2) (2008), 025701.
[10] Z.H. Chai, T.S. Zhao, A pseudopotential-based multiple-relaxation-time lattice Boltzmann model for multicomponent/multiphase flows, Acta Mech. Sin. 28 (4) (2012) 983–992.
[11] N. Looije, et al., Introducing a variable speed of sound in single-component lattice Boltzmann simulations of isothermal fluid flows, Comput. Fluids 167 (2018) 129–145.
[12] X.W. Shan, H.D. Chen, Lattice Boltzmann model for simulating flows with multiple phases and components, Phys. Rev. E 47 (3) (1993) 1815–1819.
[13] X.W. Shan, H.D. Chen, Simulation of nonideal gases and liquid-gas phase-transitions by the lattice Boltzmann-equation, Phys. Rev. E 49 (4) (1994) 2941–2948.
[14] P. Berghout, H.E.A. Van den Akker, Simulating drop formation at an aperture by means of a Multi-Component Pseudo-Potential Lattice Boltzmann model, Int. J. Heat Fluid Flow 75 (2019) 153–164.
[15] S. Mukherjee, P. Berghout, H.E.A. Van den Akker, A lattice boltzmann approach to surfactant-laden emulsions, AIChE J. 65 (2) (2019) 811–828.
[16] L. Chen, et al., A critical review of the pseudopotential multiphase lattice Boltzmann model: methods and applications, Int. J. Heat Mass Transf. 76 (2014) 210–236.
[17] K.S. Ridl, A.J. Wagner, Lattice Boltzmann simulation of mixtures with multicomponent van der Waals equation of state, Phys. Rev. E 98 (4) (2018).
[18] S. Mukherjee, et al., Simulating liquid droplets: a quantitative assessment of lattice Boltzmann and Volume of Fluid methods, Int. J. Heat Fluid Flow 70 (2018) 59–78.
[19] C. Pozrikidis, Stability of sessile and pendant liquid drops, J. Eng. Math. 72 (1) (2012) 1–20.

[20] A. Bardow, I.V. Karlin, A.A. Gusev, Multispeed models in off-lattice Boltzmann simulations, Phys. Rev. E 77 (2) (2008).
[21] E.M. Viggen, Acoustic equations of state for simple lattice Boltzmann velocity sets, Phys. Rev. E 90 (1) (2014).
[22] Y.H. Qian, Simulating thermohydrodynamics with lattice BGK models, J. Sci. Comput. 8 (3) (1993) 231–242.
[23] M.R. Kamali, et al., A multi-component two-phase lattice Boltzmann method applied to a 1-D Fischer-Tropsch reactor, Chem. Eng. J. 207 (2012) 587–595.
[24] H.R. Ashorynejad, K. Javaherdeh, H.E.A. Van den Akker, The effect of pulsating pressure on the performance of a PEM fuel cell with a wavy cathode surface, Int. J. Hydrogen Energy 41 (32) (2016) 14239–14251.
[25] N. Looije, Solution of Diffusion-reaction Equation for Varying M, 2021.

Harry Van den Akker is Bernal Professor of Fluid Mechanics at the University of Limerick, in the School of Engineering and in the Bernal Institute, while still being affiliated with Delft University of Technology as Professor of Transport Phenomena. He has supervised more than 35 PhD students in Delft and Limerick. His research interests are in multi-phase flows, turbulence and mixing, with a focus on lattice Boltzmann techniques.

Renske Donkers is a Master's student at Delft University of Technology. In her final-year research project for her Bachelor's degree in Molecular Science & Technology in 2020. She has continued her studies in the field of Chemical Engineering with a focus on computational modelling of chemical processes.

Githin Tom Zachariah is pursuing his PhD at the University of Limerick. He received his Master's degree in chemical engineering from Delft University of Technology in 2020. His research focuses on coupling Large Eddy Simulations and Direct Numerical Simulations of turbulent flows.

Orest Shardt is a lecturer in fluid mechanics and transport processes in the School of Engineering and the Bernal Institute at the University of Limerick. His research interests are in computational studies of transport phenomena, in particular in systems that involve multiphase flows. He is one of the co-authors of a textbook on lattice Boltzmann (Ref. [1]).